Soil & Tillage Research 265 (2027) 107446

Contents lists available at ScienceDirect

Soil & Tillage Research

journal homepage: www.elsevier.com/locate/still

An energy-based model of soil fragmentation by tillage

Olivier Heller [a,b,*], Andrea Carminati [b], Sara König [c], John Koestel [a], Hans-Jörg Vogel [d], Ulrich Weller [d], Thomas Keller [a,e]

[a] Agroscope, Department of Agroecology and Environment, Zürich, Switzerland
[b] ETH Zürich, Physics of Soils and Terrestrial Ecosystems, Zürich, Switzerland
[c] Federal Institute for Geosciences and Natural Ressources, Department Soil as a Resource - Properties and Dynamics, Hannover, Germany
[d] Helmholtz Centre for Environmental Research - UFZ, Soil System Science, Halle (Saale), Germany
[e] SLU, Department of Soil and Environment, Uppsala, Sweden

ARTICLE INFO

Dataset link: Dataset and Software to support "An energy-based model of soil fragmentation by tillage"

Keywords:
Atterberg limits
Unsaturated soil mechanics
Pedotransfer functions
Aggregate size distribution
Soil hydraulic properties
Specific Draught
Soil Erosion
Infiltration

ABSTRACT

Tillage greatly modifies soil structure, yet existing approaches to modelling tillage-induced soil structural change remain largely qualitative or over-simplified. Here, we present a quantitative, energy-based reformulation of the classical tillage equation that predicts soil fragmentation from the initial soil state and the applied energy. The new model partitions tillage energy into surface creation through fragmentation, displacement of existing soil fragments, and plastic deformation of the soil. Soil moisture and mechanical properties control the energy partitioning among these processes. As fragmentation progresses, an increasing proportion of tillage energy is dissipated through the displacement of existing fragments, whereas at elevated soil water contents energy is consumed by plastic deformation. Soil fragmentation resulting in the creation of new fragment surface area scales with the remaining energy. Literature-derived soil fragmentation data from drop-shatter tests and tillage experiments were used for model parameterisation. The model was subsequently evaluated against separate, independent literature datasets not used for parameterisation, covering tillage-induced soil fragmentation across a range of soil conditions. Illustrative applications demonstrate the model's ability to capture (i) the texture-dependent soil workability range and (ii) the diminishing effectiveness of repeated tillage operations. We outline how the model-derived fragment surface area can be linked to fragment size distributions under simplifying assumptions. Assuming spherical fragment geometry and a Weibull distribution of fragment sizes allows an estimation of the tillage-induced pore size distribution. Altogether, our physically grounded model provides a basis for predicting tillage-induced soil structural change and can be incorporated into agroecosystem models. Further model refinement would benefit from datasets that jointly quantify tillage energy input, soil water status, as well as pre- and post-tillage soil structure and hydraulic properties, enabling a more mechanistic description of the transition from brittle fragmentation to plastic deformation.

1. Introduction

Soil tillage is the deliberate modification of soil structure to meet the requirements of crop production (Gill and Vanden Berg, 1968; Kuipers, 1963). Its primary objectives include seedbed preparation, improvement of root growth conditions, weed control, incorporation of soil amendments, and regulation of soil water and aeration (Carter and McKyes, 2005). These objectives are achieved through soil loosening, fragmentation, mixing, and inversion, depending on the type of implement. Tillage implements can be broadly grouped into tools for primary tillage, seedbed preparation, weed control and stubble cultivation (ASABE, 2009; Bischoff et al., 2020), which differ in how strongly they induce these processes. At a fundamental level, all processes are governed by the transfer of mechanical energy from the implement to the soil.

During tillage, this energy is partitioned into (i) breaking inter-particle bonds and generating new fragment surface area, (ii) mobilising soil fragments, and (iii) plastically deforming the soil. Fragmentation increases specific fragment surface area, while fragment displacement dissipates energy through friction. Under wet conditions, a substantial proportion of the applied energy is instead consumed by plastic deformation of soil fragments (Gill and Vanden Berg, 1968). The interplay of these processes complicates a unified and predictive description of

* Corresponding author at: Agroscope, Department of Agroecology and Environment, Zürich, Switzerland.
E-mail address: olivier.heller@agroscope.admin.ch (O. Heller).

https://doi.org/10.1016/j.still.2026.107446
Received 17 April 2026; Received in revised form 18 August 2026; Accepted 19 August 2026
Available online 25 August 2026

tillage outcomes.

To conceptualise the observed behaviour, Gill and Vanden Berg (1968) introduced the so-called "tillage equation" (Eq. 1), which states that the final soil condition (S_f) can be expressed as a function of tool shape (T_s), tool motion (T_m) and the initial soil state (S_i).

$$S_f = f(T_s, T_m, S_i) \tag{1}$$

While this formulation provides a valuable conceptual framework, it remains qualitative, and the need for quantitative descriptors of both initial and final soil states has long been recognised.

Over the past decades, substantial effort has been devoted to quantifying aspects of the tillage equation. Studies have investigated soil structural changes during tillage, as summarised by Unger et al. (1982), Roytburg and Chaplin (1995), Dexter and Birkas (2004), and Obour et al. (2017). These studies show that soil properties, particularly texture and water content at the time of tillage, exert a stronger control on the resulting soil fragmentation than the details of the implement used. Sandy soils tend to fragment readily across a wide range of water contents (Müller et al., 2011). By contrast, clayey soils tilled under excessively wet conditions form large, cohesive clods, whereas they resist fragmentation due to high cohesion when dry (Ojeniyi and Dexter, 1979a; Berntsen and Berre, 1993; 2002; Keller et al., 2007). Furthermore, the efficiency of soil fragmentation is highest during the first tillage pass and decreases with successive operations (Ojeniyi and Dexter, 1979b; Berntsen and Berre., 2002). This behaviour is reflected in a log–log linear relationship between the energy required for fragmentation and fragment size (Gill and McCreery, 1960; Munkholm et al., 2002), consistent with the size-dependent likelihood of encountering pre-existing fracture planes within the soil (Dexter and Watts, 2000; Hallett and Newson, 2005). Despite these insights, a unified predictive framework is still lacking, thereby limiting the mechanistic representation of tillage-induced soil structural change in agroecosystem models.

Agroecosystem models increasingly represent changes in soil physical properties, yet soil structural dynamics are often described in an oversimplified manner. In many models, tillage effects are implemented through modification of bulk density and translated into water retention characteristics using pedotransfer functions, as reviewed by Maharjan et al. (2018), implicitly reducing structural change to a single scalar parameter. Such simplified approaches neglect that the effects of different soil structure-forming processes, such as tillage and subsequent consolidation, biopore formation by growing roots and faunal burrowing, and traffic-induced compaction, can result in different pore size distributions and pore connectivity at the same bulk density. This highlights the need to explicitly represent soil structural effects on pore size distribution and hydraulic properties (Ahuja and Green, 2022). While recently developed agroecosystem models begin to account for soil structural dynamics (König et al., 2023; Jarvis et al., 2024; Vdovenko et al., 2026), a physically consistent linkage between tillage-induced soil fragmentation and the resulting pore system characteristics remains absent. This limitation is particularly striking given that tillage represents the largest intentional geoengineering activity on Earth (Or et al., 2021). In contrast to soil consolidation, for which empirical and mechanistic models exist (Leij et al., 2002; Or and Ghezzehei, 2002), no comparable framework is available to characterise the pore size distribution resulting from tillage-induced fragmentation.

In this study, we develop, parameterise, test, and apply a parsimonious tillage model that synthesises key insights from more than six decades of research following the original formulation of the tillage equation (Eq. 1) by Gill and Vanden Berg (1968). The model is intentionally kept as simple as possible while retaining the essential mechanisms governing soil fragmentation, providing a framework that can readily be refined and extended as improved mechanistic understanding and experimental data become available. Grounded in principles of soil mechanics, the model describes fragmentation as a function of energy input and initial soil state, with parameters derived from literature data. It is applied to predict fragmentation across soils and tillage conditions, and to link fragment surface area to pore size distribution and soil hydraulic properties.

2. Model formulation

2.1. Fundamental concept

We reformulated the tillage equation (Eq. 1) to express the final specific fragment surface area (A_f [$m^2\ kg^{-1}$]) as a function of tillage energy input (W [$J\ kg^{-1}$]) and the initial soil conditions, expressed as gravimetric water content (w [$kg\ kg^{-1}$]) and initial specific fragment surface area (A_i [$m^2\ kg^{-1}$]):

$$A_f = f(W, w, A_i)\ \ [m^2\ \ kg^{-1}] \tag{2}$$

This reformulation shifts the focus from tool-specific descriptions toward an energy-based representation of soil structural change. Tool shape and motion are no longer treated as explicit predictors; their effects are implicitly accounted for through the different quantities of energy transferred to the soil by different tillage tools.

We assume that the total energy supplied to the soil during tillage (W) is partitioned among three distinct processes (Fig. 1a): plastic deformation of soil fragments (P), displacement of existing fragments (S), and fragmentation of soil into smaller fragments (E).

$$W = P + S + E\ \ [J\ \ kg^{-1}] \tag{3}$$

The relative contribution of each process depends on the initial soil state at the time of tillage: P increases with w, whereas S increases with A_i and decreases with w (Fig. 1b & c). The remaining energy, E, drives fragmentation, thereby increasing the final specific fragment surface area.

2.2. Plastic soil deformation (P)

Plastic deformation occurs when soil water content is sufficiently high for the soil to exhibit plastic rather than brittle behaviour. Classical soil mechanics identifies characteristic water contents (the shrinkage limit, the plastic limit, and the liquid limit) that delineate these regimes (Atterberg, 1911; Casagrande, 1932). Soils are brittle at water contents below the shrinkage limit, exhibit plastic behaviour at water contents above the plastic limit, and occupy an intermediate mechanical state between these limits (Harison et al., 1994).

To operationalise this concept, we introduce a water-content-dependent fraction (p) of the applied tillage energy (W) that is dissipated through plastic deformation (P). This fraction is described by a logistic function that transitions from zero to unity over the water content range between w_{SL} and w_{PL} (Eqs. 4 and 5, Fig. 1c). A scale factor ω of 15 provides a smooth transition between these consistency limits and avoids unrealistically abrupt changes in predicted tillage outcomes. Although the choice of a logistic function and the value of ω are heuristic, they represent a parsimonious approximation that can be refined if experimental data on the transition between brittle and plastic behaviour of soil become available.

$$P = p \times W\ \ [J\ \ kg^{-1}] \tag{4}$$

$$p = \begin{cases} 0 & ,\ \text{if}\ w \le w_{SL} \\ \dfrac{1}{1 + e^{\left(-\omega \times \left(\frac{w - w_{SL}}{w_{PL} - w_{SL}} - \frac{1}{2}\right)\right)}} & ,\ \text{if}\ w_{SL} < w < w_{PL} \\ 1 & ,\ \text{if}\ w \ge w_{PL} \end{cases} \tag{5}$$

where w_{SL} and w_{PL} are the water content at the shrinkage limit and the plastic limit, respectively, and p is the plastic deformation factor ranging from 0 to 1.

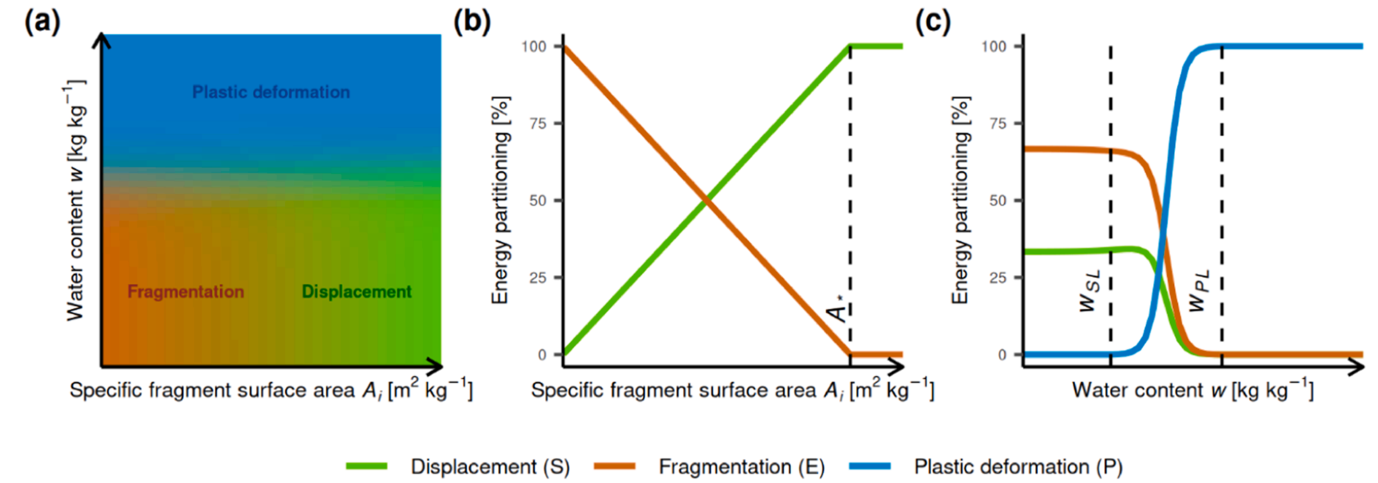

Fig. 1. Partitioning of tillage energy input into plastic deformation, displacement of fragments, and soil fragmentation depends on the soil water content (w) and initial specific fragment surface area (A_i). (a) The colour of the A_i-w-plane indicates the dominant process. A colour vision deficiency friendly version of this figure is provided as Fig. S1. (b) The effect of increasing A_i on the partitioning of an infinitesimal energy increment between fragmentation and displacement in a dry soil, where plastic deformation is negligible. A_* is a fitting parameter describing the maximum achievable specific surface area. (c) Effect of increasing w on the partitioning of an infinitesimal energy increment among all three processes for a soil with $0 < A_i < A_*$. w_{SL} and w_{PL} denote the water content at the shrinkage and the plastic limit, respectively.

2.3. *Soil fragmentation (E)*

The energy required to create new fragment surface area depends on material strength and fracture strain, both of which vary with soil texture and water content (Berntsen and Berre., 2002). Building on this knowledge, we propose an approach that derives the energy required for fragmentation directly from soil texture and water content.

The increase in specific fragment surface area ($\Delta A = A_f - A_i$ [m^2 kg^{-1}]) is assumed to scale linearly with energy available for soil fragmentation (E). The proportionality is governed by the strength of the inter-particle bonds, α [$J\ m^{-2}$], that must be overcome during fracture:

$$E = \alpha \times \Delta A = \alpha \times \left(A_f - A_i\right) \quad [J\ \ kg^{-1}] \tag{6}$$

We relate α to the apparent cohesion generated by the suction stress, σ_s [$Pa = N\ m^{-2}$], which arises from capillary forces acting at water menisci between soil particles. Apparent cohesion refers to capillary-induced bonding in unsaturated soils, whereas true cohesion denotes intrinsic inter-particle bonding that is independent of water content. For simplicity, true cohesion is neglected, and the stress required to separate soil particles, σ, is assumed to increase linearly with separation distance l up to a critical length l_{bp}, at which bond failure occurs at $\sigma = \sigma_s$ (Eq. 7).

$$\alpha = \int_{l=0}^{l_{bp}} \sigma\ dl = \sigma_s \times \frac{l_{bp}}{2} \quad [J\ m^{-2}] \tag{7}$$

2.4. *Displacement of soil fragments (S)*

As soil fragmentation progresses, the efficiency with which additional tillage energy creates new fragment surface declines, and an increasing proportion of the input energy is dissipated through the displacement of existing soil fragments rather than generating additional fragmentation. This behaviour arises because smaller fragments are more readily displaced and exhibit greater stability due to the lower probability of pre-existing fissures (Munkholm et al., 2002; Dexter and Watts, 2000; Hallett and Newson, 2005).

The energy available for fragmentation and displacement (W_{ES} [J kg^{-1}]) is given by the total tillage input energy minus the fraction dissipated through plastic deformation ($W_{ES} = E + S = W - P$). We assume that the partitioning between fragmentation (E) and displacement (S) depends on the existing specific fragment surface area (A). As only limited experimental data are currently available to constrain this partitioning, we assume an upper limit of soil fragmentation (A_*, Fig. 1b), towards which the fragmentation efficiency is progressively diminishing and ultimately approaching zero. To this end, we define the fraction of energy that contributes to creating new surface, $f_E(W_{ES})$, and the fraction that is dissipated through displacing fragments, $f_S(W_{ES})$, where $f_E(W_{ES}) + f_S(W_{ES}) = 1$. With increasing energy input W_{ES}, i.e. with increasing cumulative fragmentation, the fraction of energy consumed in the creation of new surface area is assumed to decrease according to:

$$f_E(W_{ES}) = e^{-\frac{W_{ES}}{W_*}}, \quad \text{and} \tag{8}$$

$$f_S(W_{ES}) = 1 - f_E(W_{ES}) \tag{9}$$

where W_* is the total fragmentation energy required to attain the postulated maximum specific surface area A_* beyond which all additional energy is dissipated through displacement of existing soil fragments ($W_* = A_* \times \alpha$). A_* is treated as a fitting parameter that controls the upper limit of attainable soil fragmentation (Fig. 1b). Although A_* might depend on factors such as texture, water content, and soil cohesion, the currently available experimental data are insufficient to derive a more mechanistic relationship. Future experiments should test whether A_* could be expressed as a function of measurable soil properties.

Reformulating Eq. 6, $\frac{E}{\alpha} = dA$ can be interpreted as an energy-to-surface conversion factor, so that

$$dA = \frac{1}{\alpha}\int f_E(W)\ dW \quad [m^2\ \ kg^{-1}] \tag{10}$$

This implies that the specific surface area is determined by the cumulative energy imparted to the soil during loosening. Accordingly, the relationship between the initial specific fragment surface area, A_i, and the initial energy content, W_i, is given by:

$$A_i = \int_0^{W_i} \frac{f_E(W)}{\alpha}\ dW \quad [m^2\ \ kg^{-1}] \tag{11}$$

The final specific fragment surface area after tillage, A_f, is determined by the sum of the initial specific fragment surface area, A_i, and the additional surface created by the added energy, W_{ES}:

$$A_f = \quad A_i + \int_{W_i}^{W_{ES}} \frac{f_E(W)}{\alpha} \ dW \ [m^2 \ kg^{-1}] \tag{12}$$

For operationalisation, the integral in Eq. 11 can be solved analytically and inverted to obtain W_i as a function of A_i, A_*, and α:

$$W_i = -\log\left(1 - \frac{A_i \quad \times \quad \alpha}{W_*}\right) \times W_* \\ = -\log\left(1 - \frac{A_i}{A_*}\right) \times (A_* \times \alpha) \quad [J \ kg^{-1}] \tag{13}$$

Likewise, the integral in Eq. 12 can be solved analytically to express A_f as a function of W_{ES}, W_i, A_*, and α:

$$A_f = \left(1 - e^{-\frac{W_i + W_{ES}}{W_*}}\right) \times \frac{W_*}{\alpha} \\ = \left(1 - e^{-\frac{W_i + W_{ES}}{A_* \quad \times \quad \alpha}}\right) \times A_* \ [m^2 \ kg^{-1}] \tag{14}$$

3. Model implementation, parametrisation, and validation

The model described above was implemented in R (R Core Team, 2026; Version 4.5.3) and parameterised using data compiled from the literature (Heller, 2026). All input variables and parameters contained in the model are listed in Table S1 for better overview.

3.1. Suction stress (σ_s)

Several formulations have been proposed to describe suction stress (σ_s) in unsaturated soils needed in Eq. 7, ranging from classical effective stress concepts to more recent thermodynamically based approaches (Terzaghi, 1943; Bishop, 1959; Aluko and Koolen, 2000; Alonso et al., 2013; Greco and Gargano, 2015; Lu, 2020; Salimi et al., 2021). In this study, we adopted the parsimonious formulation proposed by Bishop (1959), in which σ_s is expressed as the product of matric potential (ψ) and degree of pore saturation (χ):

$$\sigma_s(w) = \psi(w) \times \chi(w) \ [Pa] \tag{15}$$

This formulation provides a direct link between suction stress and soil hydraulic properties that can be readily derived from pedotransfer-function-based soil water retention characteristics.

In the implementation presented here, parameters for the Van Genuchten., (1980)) water retention model ($w_{saturation}$, $n_{vG}$and α_{vG}) were derived from soil texture, soil organic carbon content (*SOC*), and bulk density (ρ_b) using the pedotransfer functions of Wösten et al. (1999) and a residual water content ($w_{residual}$) of zero for all soils. If necessary, ρ_b for given combination of soil texture and *SOC* was estimated as the median of a pedotransfer-function ensemble prediction (Curtis and Post, 1964; Alexander. 1980; Federer, 1983; Huntington et al., 1989; Manrique and Jones, 1991; Tomasella and Hodnett, 1998; Bernoux et al., 1998; Men et al., 2008).

3.2. Distance between soil particles at breaking (l_{bp})

The characteristic displacement length l_{bp} required for bond failure and surface creation in Eq. 7 was inversely determined on drop-shatter test data obtained from dry soils, as under dry conditions energy losses due to plastic deformation (*P*) and fragment displacement (*S*) can be considered negligible. Consequently, the entire input energy can be assumed to be expended in the creation of new fragment surface area ($P = S = 0 \rightarrow W = E$). A value of l_{bp}= 0.2 *mm* was determined by fitting model predictions to the drop-shatter experiments conducted by Hadas and Wolf (1983) and Berntsen and Berre (1993). The close agreement between the measured and predicted values across different soil textures (Fig. 2) indicates that this l_{bp} value provides a consistent representation of soil fracture behaviour under dry conditions.

3.3. Maximum specific fragment surface area ($\boldsymbol{A_*}$)

Inverse determination of the maximum specific fragment surface area (A_*) above which all additional energy is dissipated through fragment displacement (Eqs. 13 and 14), using data from Berntsen and Berre (1994) and, (2002), yielded a value of $A_* = 6 \ m^2 \ kg^{-1}$(Fig. 3). For a homogeneous assembly of spherical soil fragments with a density of 1500 $kg \ m^{-3}$, this corresponds to a characteristic fragment diameter of approximately $\frac{2}{3}$ *mm*, suggesting that the obtained A_* represents a typical upper limit of fragmentation achievable under field conditions in arable topsoils.

3.4. Transition from brittle to plastic behaviour (w_{SL} and w_{PL})

The transition from plastic to brittle mechanical behaviour is expected to occur between the plastic limit and the shrinkage limit of a soil. This transition is represented in Eq. 5 by two soil-specific water contents (w_{SL}, w_{PL}), of which w_{PL} was operationally defined by Dexter and Bird (2001):

$$w_{PL} = w_{inflect} + 0.4 \times \left(w_{saturation} - w_{inflect}\right) \ [kg \ kg^{-1}] \tag{16}$$

The w_{PL} corresponds to the onset of substantial air entry into the pore system and marks a rapid decline in pore saturation (Dexter and Bird, 2001). The inflection point of the water retention curve ($w_{inflect}$) was determined from the van Genuchten parameters. We defined the shrinkage limit (w_{SL}) symmetrically with respect to the inflection point of the water retention curve and the residual water content (Eq. 17).

$$w_{SL} = w_{inflect} - 0.4 \times \left(w_{inflect} - w_{residual}\right) \ [kg \ kg^{-1}] \tag{17}$$

Together, w_{PL} and w_{SL} delineate the part of the water retention curve over which changes in water content per unit change in matric potential are greatest and approximately linear (Fig. 4). This region corresponds to the progressive drainage of structural pores and is therefore associated with pronounced changes in soil mechanical behaviour (Dexter and Bird, 2001). We found good agreement between w_{SL} and w_{PL} derived with Eqs. 16 and 17, and pedotransfer-function-derived estimates of the Atterberg limits (Keller and Dexter, 2012; Knadel et al., 2021; Krabbe, 1958; Mucha and Wójcik, 2013) across all textural classes (Fig. S2).

3.5. Validation against independent data

To evaluate the parametrised model, we collated an independent meta-database, comprising datasets not used for model parameterisation, on tillage-induced soil fragmentation from the literature (Fig. 5). Specifically, we collected data on energy input (*W*), resulting specific fragment surface area (A_f), soil texture, *SOC*, and *w* from three published studies. In total, these studies comprised 72 combinations of tillage operations and soil conditions.

Initial comparison of measured and predicted surface areas (Fig. 5a) revealed that the model in general predicted qualitative trends correctly. However, the model systematically overestimated fragment surface area in the two Swedish studies that contributed most observations (Arvidsson et al., 2004; Arvidsson and Hillerström, 2010). This discrepancy can be attributed to methodological differences: in the Swedish studies, surface area was calculated from fragment size distributions using a minimum sieve size of 4 *mm*, whereas the datasets used for model parametrisation resolved fragment sizes down to 0.5 *mm*. Consequently, a substantial fraction of the fragment surface area was not captured in the Swedish measurements. To account for this systematic truncation, the reported surface areas were scaled by a constant factor of eight. This factor reflects the eightfold difference in minimum resolved

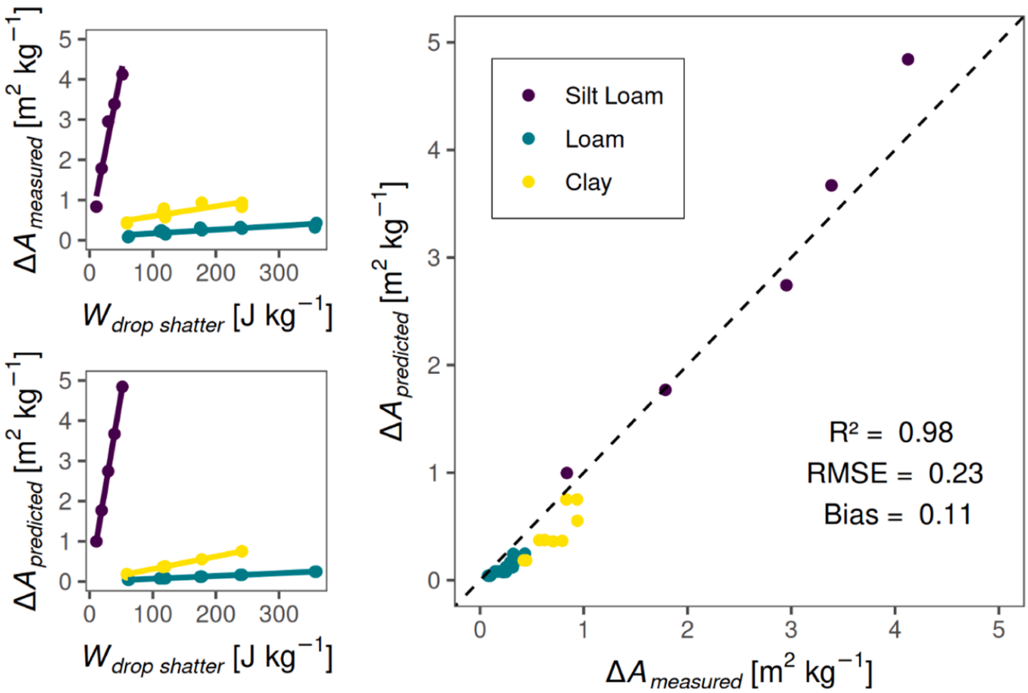

Fig. 2. Comparison of measured and predicted ΔA from drop-shatter tests for three soils across increasing energy input $W_{drop\ shatter}$. Predictions were obtained using Eqs. 6 and 7 with an l_{bp} of 0.2 *mm*. Silt loam denotes a soil with 25% *clay*, 55% *silt*, 1% *SOC*, a bulk density (ρ_b) of 1400 $kg\ m^{-3}$, and a gravimetric water content (w) of 0.16 $kg\ kg^{-1}$ (Berntsen and Berre, 1993). Loam denotes a soil with 27% *clay*, 44% *silt*, 0.1% *SOC*, ρ_b of 1450 $kg\ m^{-3}$, and w of 0.043 $kg\ kg^{-1}$ (Hadas and Wolf, 1983). Clay denotes a soil with 47% *clay*, 16% *silt*, 0.6% *SOC*, ρ_b of 1450 $kg\ m^{-3}$, and w of 0.107 $kg\ kg^{-1}$ (Hadas and Wolf, 1983).

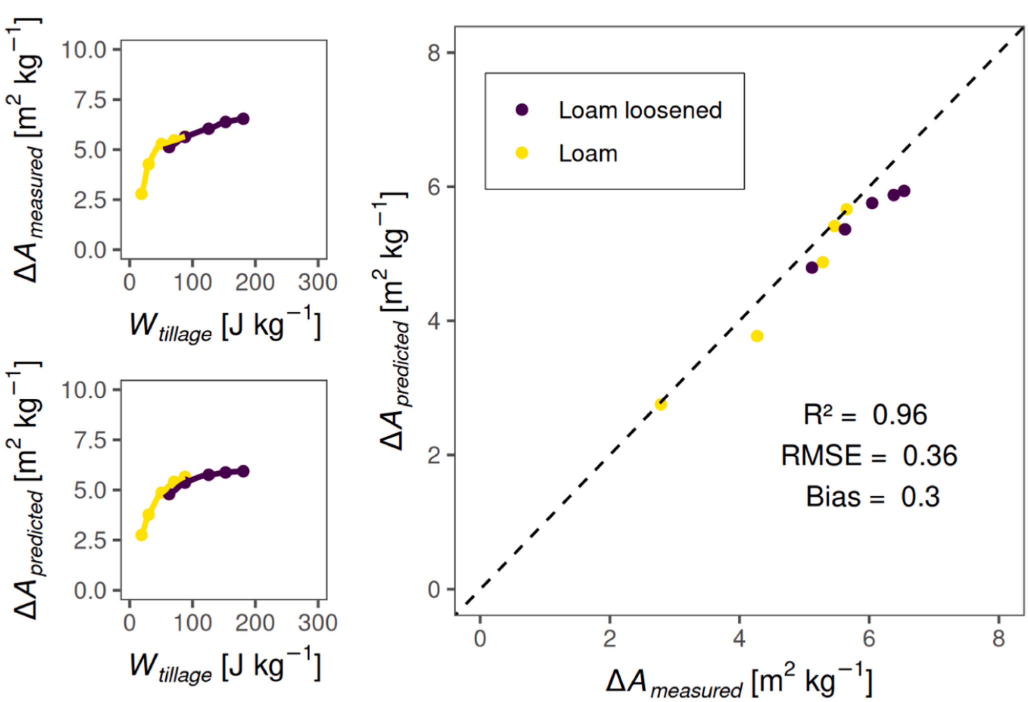

Fig. 3. Comparison of measured and predicted ΔA across increasing energy inputs $W_{tillage}$ during multiple tillage passes for two soils. Predictions were obtained using $A_* = 6\ m^2\ kg^{-1}$. Loam denotes a soil with 24% *clay*, 44% *silt*, 1% *SOC*, a bulk density (ρ_b) of 1366 $kg\ m^{-3}$, and gravimetric water content (w) of 0.17 $kg\ kg^{-1}$. Loam loosened denotes the same soil in a loosened state, i.e. at ρ_b of 1409 $kg\ m^{-3}$ and w of 0.15 $kg\ kg^{-1}$. All data are from Berntsen and Berre (1994) and, (2002).

fragment diameter and the fact that specific surface area scales inversely with fragment diameter for geometrically similar particles of constant density. We note, however, that the factor of eight should be interpreted as a pragmatic correction, not as an exact transformation of the total fragment surface area. A rigorous correction would require detailed knowledge of the fragment size distribution, which was not consistently available in the reported datasets, necessitating a simplified scaling approach. Following this adjustment, modelled and measured surface areas showed reasonable agreement across soils and tillage operations (Fig. 5b), indicating that the model reproduces the overall magnitude

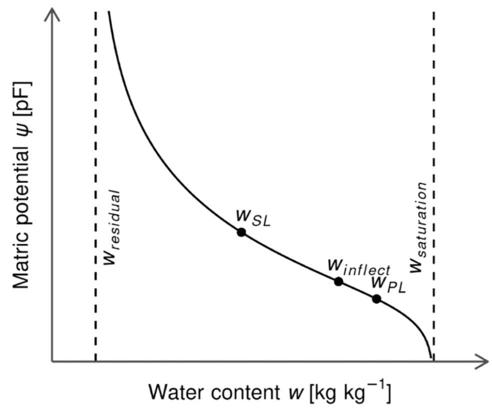

Fig. 4. Generic soil water retention curve, indicating the residual water content ($w_{residual}$), shrinkage limit (w_{SL}), inflection point ($w_{inflect}$), plastic limit (w_{PL}), and saturated water content ($w_{saturation}$).

and major trends of tillage-induced soil fragmentation across independent datasets, although methodological differences among the underlying studies limit a rigorous quantitative validation. Additional analyses of the validation data revealed no consistent dependence of the prediction error on soil texture, SOC, ρ_b, or W. The most consistent pattern was observed for soil moisture, where the model tended to underestimate the specific fragment surface area created under wet conditions (Fig. S3). Consistent with this observation, model performance declined with increasing soil water content, as reflected by the larger RMSE for wet soil compared with the dry and moist soils (Fig. S4). These results suggest that refinement of the representation of the transition between brittle fragmentation and plastic deformation (i.e. Eqs. 4, 5, 16, or 17) should be prioritised before introducing additional complexity into other parts of the model.

4. Model application

We applied the parametrised and tested model to evaluate whether it can reproduce phenomena observed by farmers and documented in the literature (see introduction). The first example was chosen to showcase the model's capability to reproduce different tillage outcomes due to soil texture and water content. The second example investigates how the model predicts the efficacy of the first and subsequent tillage operations.

4.1. Optimal soil workability range across soil texture classes

The model was applied to predict the minimum energy input required to achieve an adequate seedbed across different soil textures and water contents. Based on these predictions, we derived the soil workability range, defined here as the range of water contents within which a satisfactory tillage outcome can be achieved with a realistic energy input of ≤ 150 J kg^{-1} (see Fig. S5 based on the data from Hadas and Wolf (1983), Berntsen and Berre., (2002), Arvidsson et al. (2004), and Arvidsson and Hillerström (2010)). A target specific fragment surface area of 3 m^2 kg^{-1} was used as a criterion for a well-fragmented seedbed. This target value corresponds to soil fragments that follow a Weibull distribution (see Section 5.1) with a mean weight diameter of 10 *mm*, a value that Berntsen and Berre., (2002)) considered to constitute a good seedbed. The minimum energy input required to reach this target surface area was calculated for the twelve USDA textural classes across the full range of water contents.

The resulting predictions (Fig. 6a) demonstrate strong dependence on both soil texture and water content, with the highest energy requirements and the narrowest soil workability range observed in clay-rich soils. The increase in tillage energy requirement with increasing clay content is reflected in the higher draught forces required for tillage of fine-textured soils (ASABE, 2011). Such fine-textured soils are often referred to by German-speaking practitioners as "Minutenböden" ("minute soils") highlighting the narrow water content window within which these soils are suitable for tillage. The narrowing of the soil workability range with increasing clay content is consistent with observations by Dexter and Bird (2001) and is reflected in the soil workability chart shown in Fig. 6b originally presented by Petelkau (1984). The model reproduces the narrowing soil workability range with increasing clay content well. However, the predicted soil workability ranges seem to be biased to towards wetter soil conditions (i.e. toward the right if Fig. 6b). Additionally, the model tends to under- and overestimate the workability at high water contents depending on soil

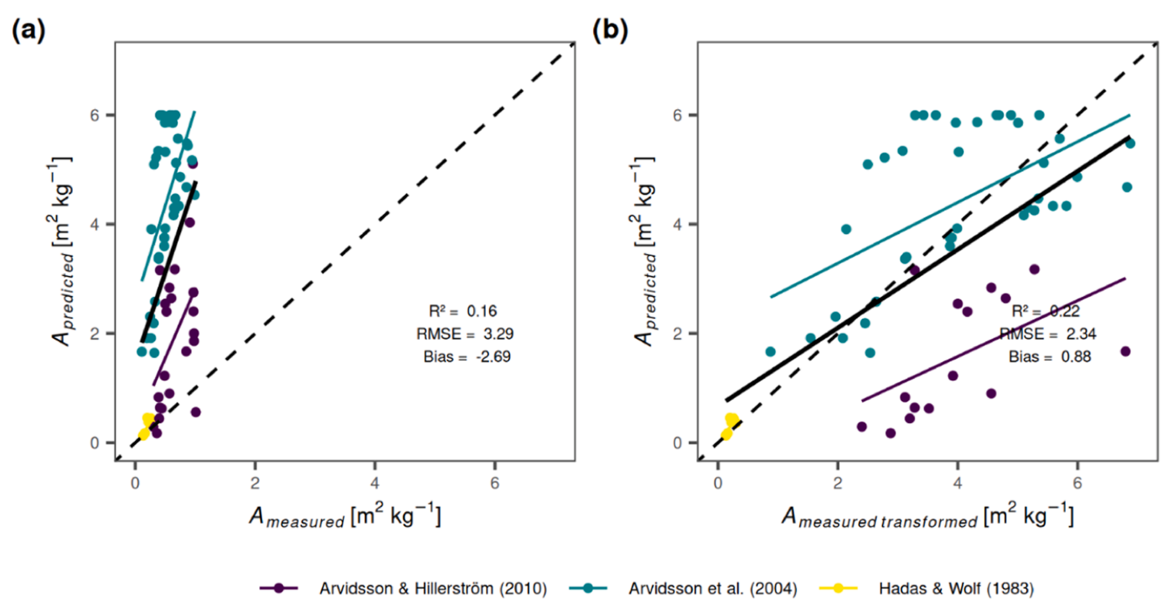

Fig. 5. (a) Comparison of literature-derived ($A_{measured}$) and predicted specific fragment surface area ($A_{predicted}$) after tillage operations. (b) The literature-derived measured surface area was transformed to account for methodological differences ($A_{measured\ transformed}$).The colours indicate the study where the measured data were reported, solid lines represent the regression line of either all data or the data from each source separately, and the dashed lines are the 1:1 line. RMSE refers to root mean square error, a measure of the distances between observed and predicted values.

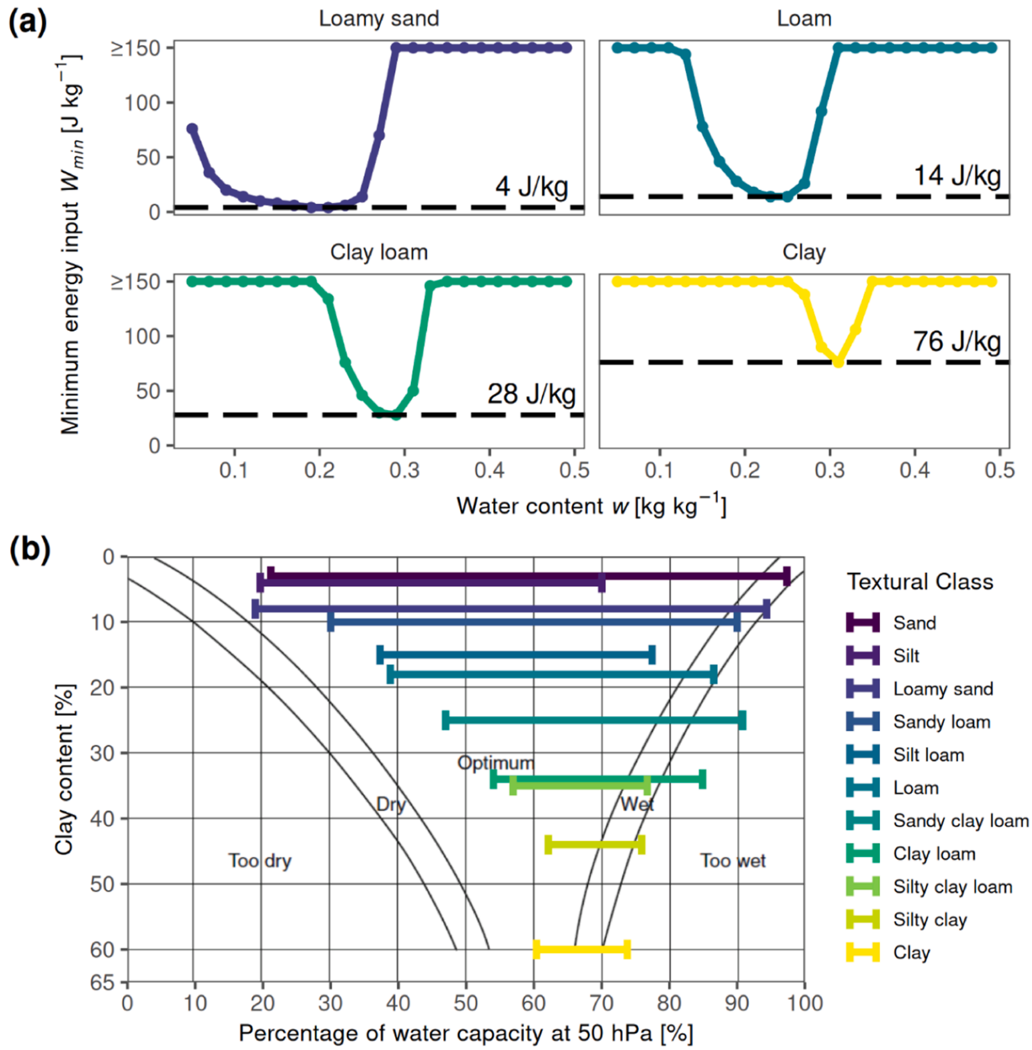

Fig. 6. Predictions of soil workability ranges across soil textures. (a) Minimum energy required to produce a seedbed with a specific fragment surface area of 3 m^2 kg^{-1} for four soil textures, as a function of water content. (b) Comparison of the model-predicted soil workability ranges with the empirical soil workability chart of Petelkau (1984), obtained from Müller et al. (2011), which defines water content ranges suitable for tillage relative to the water content at field capacity (defined by Petelkau 1984 as a matrix suction of 50 hPa). The model-derived soil workability range is defined as the range of water contents for which a specific fragment surface area of 3 m^2 kg^{-1} can be achieved with an energy input of ≤ 150 J kg^{-1}. Sandy clay soils are omitted to reduce overlap among textural classes and improve clarity.

textural composition. Particularly the wet end of the workability range of silt-rich soils (Silt, Silt loam) are predicted to be at lower water content compared to the soil workability chart. This observation is consistent with the validation results presented in Figs. S3 and S4, which indicate sharply increasing relative prediction errors as the water content approaches the soils plastic limit. Our model nevertheless provides a mechanistic basis supporting the empirical soil-workability chart, reproducing a narrow soil workability range for clayey soils, and a much wider range for sandy soils, spanning nearly the entire water content range below field capacity.

4.2. Diminishing efficacy of successive tillage operations

Repeated harrowing operations are sometimes applied to create a suitable seedbed for crops. Ojeniyi and Dexter., (1979b)) as well as Berntsen and Berre., (2002)) documented progressively smaller increases in soil fragment surface area with subsequent operations. Our model reproduces this characteristic decline in tillage efficacy (Fig. 7a). In the example shown, the first tillage pass produced the largest increase in specific surface area (3.2 m^2 kg^{-1}). Whereas the second and the third pass increasingly dissipated energy through displacement of fragments rather than through the creation of new surface area (Fig. 7b) and only produced an additional surface of 1.3 and 0.6 m^2 kg^{-1}, respectively. The proportions of these values correspond well with Berntsen and Berre (1994) who reported an increase of 2.8, 1.5 and 1.0 m^2 kg^{-1} for the first, second, and third pass respectively. In the model, this decreasing breaking efficiency of additional energy (Fig. 7c) is a direct consequence of the dependence of energy partitioning to fragment displacement on the existing surface area, without requiring any explicit representation of tillage history. This behaviour provides a physically based explanation for the limited effectiveness of repeated tillage operations and, in combination with Fig. 6, underscores that tillage timing with respect to soil water content is more critical than increasing the number of passes to achieve a good seedbed.

5. Model extension to predict fragment size distribution and pore size distribution

5.1. Weibull distribution of tillage fragments

Representing soil structural dynamics following tillage in agroecosystem models is important because it enables simulation of changes

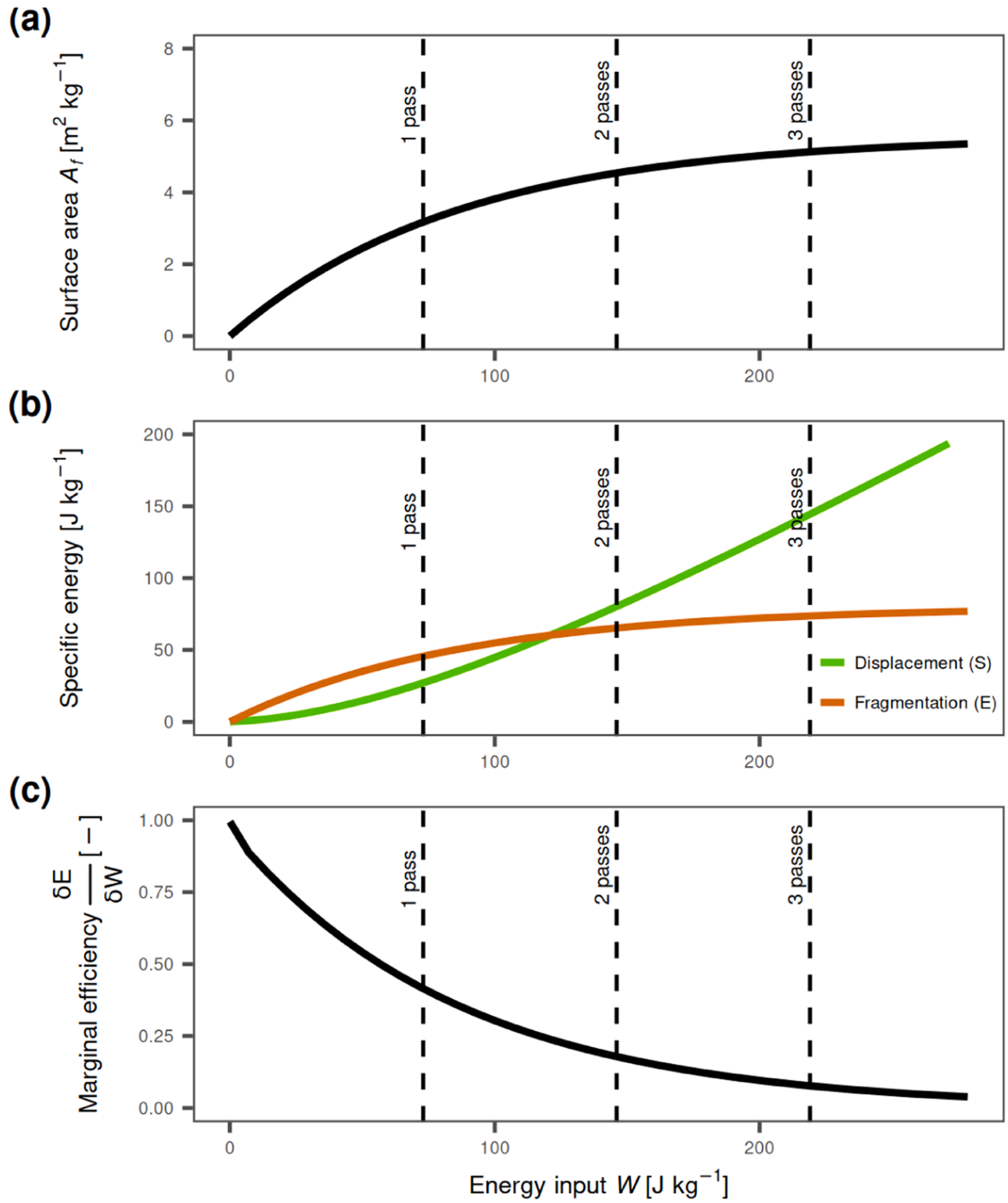

Fig. 7. (a) Simulated specific fragment surface area (A_f) as a function of tillage energy inputs (W). (b) Partitioning of the energy input into the two processes of fragmentation and displacement. (c) The marginal fragmentation efficiency of an additional quantity of energy input. The marginal efficiency is calculated as the ratio of the increase in energy partitioned to fragmentation divided by the increase in input energy. (a-c) Dashed lines indicate the characteristic energy input for one to three successive disc operations during seedbed preparation. The simulated soil had a texture of 30% *clay* and 25% *silt*, with a water content of 0.15 $kg\ kg^{-1}$ that is dry enough that plastic deformation is negligible.

in soil hydraulic properties, which control the partitioning between infiltration and runoff and are therefore key predictors in both crop and erosion modelling (Chandrasekhar et al., 2018). The proposed model provides a quantitative estimate of the resulting specific fragment surface area, which can serve as a basis for representing these tillage induced structural changes. The predicted surface areas can be translated into a soil fragment size distribution by assuming a Weibull distribution of fragment mass (Eq. 18; Perfect et al., 1993). The Weibull 2-parameter distribution provides sufficient flexibility to represent a wide range of fragment size spectra while being mathematically tractable. The distribution is defined by a shape and scale parameter (k and λ, respectively).

$$M(x) = \frac{k}{\lambda}\left(\frac{x}{\lambda}\right)^{k-1}\exp\left[-\left(\frac{x}{\lambda}\right)^{k}\right]\quad [kg\ kg^{-1}] \tag{18}$$

We fitted two-parameter Weibull distributions to 97 fragment size distribution datasets reported in the literature (Keller et al., 2007; Álvaro-Fuentes et al., 2008; Hevia et al., 2007; Adem et al., 1984) to establish a unique link between specific surface area and fragment size distribution. This analysis yielded a relatively narrow distribution for the shape parameter k with a mean of = 0.71 and a SD of 0.29 (Fig. S6). However, a Weibull distribution with $k < 1$ implies an infinitely large proportion of fragments with zero diameter, which is physically impossible and leads to numerical instability in the calculation of the specific fragment surface area with Eq. 19. To obtain a physically meaningful and robust representation, the shape parameter was therefore fixed at $k = 1.1$. This value is close to but greater than one, retaining a distribution where the small fragments dominate the distribution while ensuring a finite probability density for small fragments. This choice of k is not critical, as the resulting scale parameter λ was found to be largely insensitive to the exact value of k (Fig. S6). Fixing k in this way enables a unique relationship between specific surface area (A) and fragment size distribution. Under the assumption of spherical fragment geometry, the specific surface area can then be calculated from the Weibull distribution (Eq. 19).

$$A = \int_0^\infty \left(\frac{M(x)}{\rho_f} \times \frac{6}{x}\right) dx \ [m^2 \ kg^{-1}] \tag{19}$$

Eqs. 18 and 19 allow to numerically obtain the scale parameter λ of the Weibull distribution for a given A, fragment density (ρ_f), and a fixed k. Simulations across a wide range of A and ρ_f revealed a log-log-linear relationship between A and λ (Fig. 8).

The relationship observed in Fig. 8 was approximated using a regression-based meta-model (Eq. 20), providing a computationally efficient means of deriving fragment size distributions from predicted specific fragment surface area:

$$log_{10}(\lambda(A, \rho_f)) = a \quad + \quad b \times log_{10}(A) \quad + \quad c \ \frac{1}{\rho_f} \tag{20}$$

where a, b and c were found to be -1.765, -1.000 and 575.3 respectively ($R^2 = 1.00$).

5.2. Size distribution of inter-fragment pore space

From the Weibull size distribution of soil fragments, the void ratio (e) of the fragmented soil was estimated as (Brouwers, 2016):

$$e = e_1 * \exp\left(-2\sqrt{\pi}(1 - e_1)\frac{\beta}{k}\right) \ [m^3 \ m^{-3}] \tag{21}$$

where e_1 is the monosized void ratio and β is the contraction coefficient. For random loose packed spheres, e_1 and β are 0.45 and 0.16, respectively (Brouwers, 2016), leading to a calculated void ratio e of 0.34. This e corresponds to an approximate bulk density reduction of one third, a value consistent with assumptions commonly adopted in soil–-crop models such as EPIC (Williams et al., 1984).

Finally, the inter-fragment pore size distribution was derived from the fragment size distribution and e using an adapted form of the approach of Arya and Paris (1981):

$$V_i = \frac{m_i}{\rho_f} \times e \ [m^3] \tag{22}$$

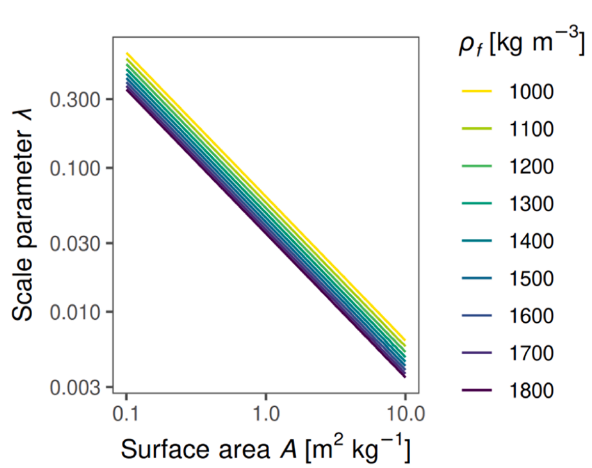

Fig. 8. Simulation results of the Weibull scale parameter (λ) with Eqs. 18 and 19 as a function of specific surface area (A) and fragment density (ρ_f) for a fixed Weibull shape parameter $k = 1.1$. The results of the simulation were approximated with a regression-based meta-model (Eq. 20).

$$r_i = R_i \times \sqrt{\frac{4 \ e \, n_i^{1-\beta}}{6}} \ [m] \tag{23}$$

where V_i is the pore volume that corresponds to the i-th fragment size class, m_i is the total mass of the size class, e is the void ratio and ρ_f is the density of the soil fragments. The mean radius of each pore size class (r_i) depends on the mean radius of the corresponding soil fragments (R_i) and the number of soil fragments in that class (n_i). The empirical constant β was set to 1.38 (Arya and Paris, 1981; Gupta et al., 1991).

Although originally developed to relate particle size distributions to soil water retention characteristics, the Arya and Paris (1981) approach has also been applied to fragmented soil structures (Gupta and Ewing, 1989; Gupta et al., 1991; Hassan et al., 2022). The resulting pore size distributions (Fig. 9) represent the inter-fragment pore space, with changes in intra-fragment porosity not explicitly captured. They nevertheless enable prediction of the water retention characteristics of the inter-fragment pore system and thereby provide a direct pathway for integrating the proposed tillage model into agroecosystem and soil erosion models.

6. Summary and outlook

In this study, we revisited the classical tillage equation (Eq. 1) and proposed a quantitative, energy-based model that predicts soil fragmentation from the initial soil state and the applied mechanical energy. By partitioning tillage energy into contributions for surface area creation, plastic deformation, and displacement of soil fragments, the framework provides a physically consistent link between soil water content, mechanical behaviour, and structural outcomes. The model reproduces empirical observations, including the strong dependence of fragmentation efficiency on soil water content, the narrow water content range suitable for tillage observed in clayey soils, and the diminishing effectiveness of repeated tillage operations. The proposed model focuses deliberately on the immediate structural consequences of tillage, without representing soil consolidation. Coupling the model with consolidation models, such as those of Or and Ghezzehei (2002) or Leij et al. (2002), as implemented by Chandrasekhar et al. (2019), represents a promising avenue for future development.

Although the model was parameterised and independently evaluated using existing datasets, the available data do not permit a rigorous quantitative validation across soil and tillage conditions. Datasets in which tillage energy input, soil water content, fragment size distributions, and soil hydraulic properties are measured simultaneously remain limited. The validation results indicate that the current model captures fragmentation behaviour well under relatively dry conditions but fails to correctly predict fragmentation at water contents close to the soils plastic limit. Targeted experiments across different soil textures could provide the data needed to further test and refine the proposed model. Such efforts should aim to improve the representation of the transition from brittle fragmentation of dry soil to plastic deformation of wet soil, as well as to better characterise the soil properties governing the energy partitioning between fragment creation and fragment displacement.

Finally, the proposed framework provides a mechanistic pathway for linking tillage-induced structural change to pore size distributions and soil hydraulic properties. This establishes a basis for simulating the effects of tillage on water flow, gas transport, organic matter turnover, and soil erosion within process-based agroecosystem models.

CRediT authorship contribution statement

Andrea Carminati: Writing – review & editing, Supervision, Investigation, Conceptualization. **Sara König:** Writing – review & editing, Supervision, Conceptualization. **John Koestel:** Writing – review & editing, Conceptualization. **Hans-Jörg Vogel:** Writing – review & editing, Writing – original draft, Validation, Investigation,

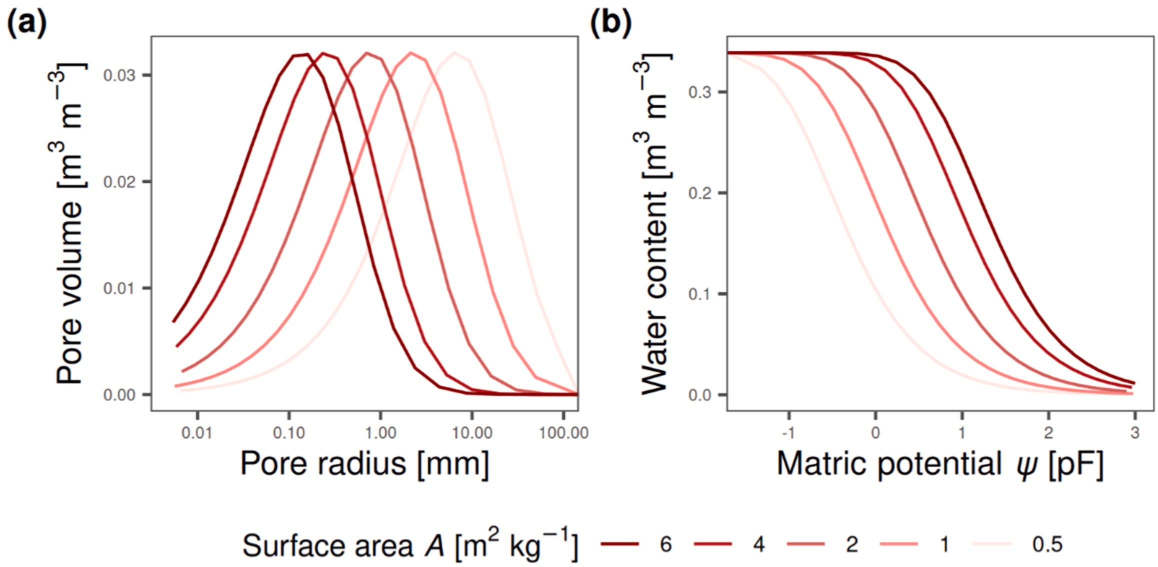

Fig. 9. (a) Size distribution of inter-fragment pores at different specific surface areas (A) were predicted with Eqs. 20–23. Lower A values correspond to larger soil fragments and larger inter-fragment pores in the soil following tillage. (b) The pore size distribution depicted in (a) can be converted into water retention characteristics of the tillage-induced inter-fragment pore space using the capillary law of Jurin (1719).

Conceptualization. **Olivier Heller:** Writing – original draft, Visualization, Validation, Software, Methodology, Investigation, Formal analysis, Data curation, Conceptualization. **Ulrich Weller:** Writing – review & editing, Validation, Investigation, Conceptualization. **Thomas Keller:** Writing – review & editing, Writing – original draft, Visualization, Validation, Supervision, Investigation, Conceptualization.

Declaration of Generative AI and AI-assisted technologies in the writing process

During the preparation of this work, the authors used GitHub CoPilot to support software development, and ChatGPT to improve language and readability of the manuscript. All content was reviewed and edited by the authors, who take full responsibility for the accuracy and integrity of the published article.

Declaration of Competing Interest

The authors declare the following financial interests/personal relationships which may be considered as potential competing interests: Prof. Thomas Keller was Editor of Soil and Tillage Research and is co-author of this article. All other authors declare that they have no known competing financial interests or personal relationships that could have appeared to influence the work reported in this paper.

Acknowledgments

We thank Dr. Rolf Berntsen (former Agricultural University of Norway, Ås, Norway), Prof. em. Sathish Gupta (University of Minnesota, Minnesota, United States of America) and Prof. em. Ed Perfect (University of Tennessee, Knoxville, United States of America) for the helpful and supportive exchange while developing the presented model. Furthermore, we are grateful for the support in literature search by Ursula Bürkli and Aristidis Harissiadis from ETH Zurich Library (Switzerland), Martina Gubser from Agroscope Documentary Service (Switzerland), Kurt Spokas and Ann Perry from USDA-ARS (United States of America), Bendik Egner from the Library of the Norwegian University of Life Sciences (Norway), Sebastian Ineichen from Berne University of Applied Science (Switzerland), and Kate McManus from University of Minnesota Libraries (United States of America).

Data availability statement

All data and software to support this study are available on Zenodo (Heller, 2026) and Gitlab (https://gitlab.com/heoi/tillage-model).

Appendix A. Supporting information

Supplementary data associated with this article can be found in the online version at doi:10.1016/j.still.2026.107446.

Data availability

Research Link Provided

Dataset and Software to support "An energy-based model of soil fragmentation by tillage" (Zenodo)

References

Adem, H.H., Tisdall, J.M., Willoughby, P., 1984. Tillage management changes size-distribution of aggregates and macro-structure of soils used for irrigated row-crops. Soil. Tillage Res. 4 (6), 561–576. https://doi.org/10.1016/0167-1987(84)90005-9.

Ahuja, L.R., Green, T.R., 2022. Quantifying and modeling management effects on soil properties: tillage, reconsolidation, crop residues, and crop management. Model. Process. Their Interact. Crop. Syst. Chall. 21st Century 333–358. https://doi.org/10.1002/9780891183860.ch11.

Alexander, E.B., 1980. Bulk densities of California soils in relation to other soil properties. Soil. Sci. Soc. Am. J. 44 (4), 689–692. https://doi.org/10.2136/sssaj1980.03615995004400040005x.

Alonso, E.E., Pinyol, N.M., Gens, A., 2013. Compacted soil behaviour: initial state, structure and constitutive modelling. Géotechnique 63 (6), 463–478. https://doi.org/10.1680/geot.11.P.134.

Aluko, O.B., Koolen, A.J., 2000. The essential mechanics of capillary crumbling of structured agricultural soils. Soil. Tillage Res. 55 (3), 117–126. https://doi.org/10.1016/S0167-1987(00)00105-7.

Álvaro-Fuentes, J., Arrúe, J.L., Cantero-Martínez, C., López, M.V., 2008. Aggregate breakdown during tillage in a mediterranean loamy soil. Soil. Tillage Res. 101 (1–2), 62–68. https://doi.org/10.1016/j.still.2008.06.004.

Arvidsson, J., Hillerström, O., 2010. Specific draught, soil fragmentation and straw incorporation for different tine and share types. Soil. Tillage Res. 110 (1), 154–160. https://doi.org/10.1016/j.still.2010.07.003.

Arvidsson, J., Keller, T., Gustafsson, K., 2004. Specific draught for mouldboard plough, chisel plough and disc harrow at different water contents. Soil. Tillage Res. 79 (2), 221–231. https://doi.org/10.1016/j.still.2004.07.010.

Arya, Lalit M., Paris, Jack F., 1981. A PhysicoEmpirical Model to Predict the Soil Moisture Characteristic from Particle-size Distribution and Bulk Density Data. Soil. Sci. Soc. Am. J. 45 (6), 1023–1030. https://doi.org/10.2136/sssaj1981.03615995004500060004x.

ASABE, 2011. Agricultural Machinery Management Data. ASAE Data D497.7. American Society of Agricultural Biological Engineers, St. Joseph, MI. https://elibrary.asabe.org/abstract.asp?aid=36431.

ASABE. 2009. Terminology and Definitions for Agricultural Tillage Implements. ASAE Standard S414.2. St. Joseph, MI: American Society of Agricultural Biological Engineers. https://elibrary.asabe.org/abstract.asp?aid=44205.

Atterberg, Albert, 1911. Die Plastizität der Tone. Int. Mitt. für Bodenkd. 1 (1), 10–43.

Bernoux, Martial, Cerri, Carlos, Arrouays, Dominique, Jolivet, Claudy, Volkoff, Boris, 1998. Bulk densities of brazilian amazon soils related to other soil properties. Soil. Sci. Soc. Am. J. 62 (3), 743–749. https://doi.org/10.2136/sssaj1998.03615995006200030029x.

Berntsen, R., Berre, B., 1993. Fracturing of soil clods and the soil crumbling effectiveness of draught tillage implements. Soil. Tillage Res. 28 (1), 79–94. https://doi.org/10.1016/0167-1987(93)90057-V.

Berntsen, R., and B. Berre. 1994. "Crumbling Efficiency of Various Implements." In International Soil Tillage Research Organization, Proceedings of 13th International Conference, Aalborg, Denmark, 1221–26.

Berntsen, R., Berre, B., 2002. Soil fragmentation and the efficiency of tillage implements. Soil. Tillage Res. 64 (1), 137–147. https://doi.org/10.1016/S0167-1987(01)00251-3.

Bischoff, Joachim, Joachim Brunotte, Johannes Buhl, J. Denger, Markus Demmel, Detlev Dölger, Detlef Ehlert, et al. 2020. "Soil Cultivation and Sowing - Definitions of Soil Cultivation and Sowing System." Kuratorium für Technik und Bauwesen in der Landwirtschaft e.V. (KTBL).

Bishop, Alan W., 1959. "The principal of effective stress.". Tek. Ukebl. 39 (106), 859–863.

Brouwers, H.J.H., 2016. Packing fraction of particles with a weibull size distribution. Phys. Rev. E 94 (1). https://doi.org/10.1103/physreve.94.012905.

Carter, M.R., McKyes, E., 2005. Cultivation and tillage. In: Daniel, Hillel (Ed.), Encyclopedia of Soils in the Environment. Elsevier, Oxford, pp. 356–361. https://doi.org/10.1016/B0-12-348530-4/00514-2.

Casagrande, Arthur, 1932. "Research on the atterberg limits of soils. Public Roads 13 (8), 121–136.

Chandrasekhar, P., Kreiselmeier, J., Schwen, A., Weninger, T., Julich, S., Feger, K.H., Schwärzel, K., 2018. Why we should include soil structural dynamics of agricultural soils in hydrological models. Water 10 (12), 1862. https://doi.org/10.3390/w10121862.

Chandrasekhar, Parvathy, Kreiselmeier, Janis, Schwen, Andreas, Weninger, Thomas, Julich, Stefan, Feger, Karl-Heinz, Schwärzel, Kai, 2019. Modeling the evolution of soil structural pore space in agricultural soils following tillage. Geoderma 353, 401–414. https://doi.org/10.1016/j.geoderma.2019.07.017.

Curtis, Robert O., Post, Boyd W., 1964. Estimating bulk density from organic-matter content in some vermont forest soils. Soil. Sci. Soc. Am. J. 28 (2), 285–286. https://doi.org/10.2136/sssaj1964.03615995002800020044x.

Dexter, A.R., Bird, N.R.A., 2001. Methods for predicting the optimum and the range of soil water contents for tillage based on the water retention curve. Soil. Tillage Res. 57 (4), 203–212. https://doi.org/10.1016/s0167-1987(00)00154-9.

Dexter, A.R., Birkas, M., 2004. Prediction of the soil structures produced by tillage. Soil. Tillage Res. 79 (2), 233–238. https://doi.org/10.1016/j.still.2004.07.011.

Dexter, A.R., Watts, Chris W., 2000. Tensile strength and friability. Soil and Environmental Analysis. CRC Press, pp. 417–446.

Federer, C.A., 1983. Nitrogen mineralization and nitrification: depth variation in four new england forest soils. Soil. Sci. Soc. Am. J. 47 (5), 1008–1014. https://doi.org/10.2136/sssaj1983.03615995004700050034x.

Gill, W.R., McCreery, W.F., 1960. "Relation of size of cut to tillage tool efficiency.". Agric. Eng. 41 (6), 372–381.

Gill, W.R., Vanden Berg, G.E.., 1968. *Soil Dynamics in Tillage and Traction*. Agricultural Handbook. 316. Agricultural Research Service, USDA.

Greco, Roberto, Gargano, Rudy, 2015. A novel equation for determining the suction stress of unsaturated soils from the water retention curve based on wetted surface area in pores. Water Resour. Res. 51 (8), 6143–6155. https://doi.org/10.1002/2014wr016541.

Gupta, S.C., and R.P. Ewing. 1989. "Modeling Water Retention Characteristics and Surface Roughness of Tilled Soils." In Indirect Methods for Estimating the Hydraulic Properties of Unsaturated Soils. Proceedings of the International Workshop on Indirect Methods for Estimating the Hydraulic Properties of Unsaturated Soils. Riverside, California, 379–388.

Gupta, S.C., Lowery, B., Moncrief, J.F., Larson, W.E., 1991. Modeling tillage effects on soil physical properties. Soil. Tillage Res. 20 (2), 293–318. https://doi.org/10.1016/0167-1987(91)90045-Y.

Hadas, A., Wolf, D., 1983. Energy efficiency in tilling dry clod-forming soils. Soil. Tillage Res. 3 (1), 47–59. https://doi.org/10.1016/0167-1987(83)90016-8.

Hallett, P.D., Newson, T.A., 2005. Describing soil crack formation using elastic–plastic fracture mechanics. Eur. J. Soil. Sci. 56 (1), 31–38. https://doi.org/10.1111/j.1365-2389.2004.00652.x.

Harison, Jack A., Hardin, Bobby O., Mahboub, Kamyar, 1994. Fracture toughness of compacted cohesive soils using ring test. J. Geotech. Eng. 120 (5), 872–891. https://doi.org/10.1061/(ASCE)0733-9410(1994)120:5(872).

Hassan, S.B., Dragonetti, G., Comegna, A., Sengouga, A., Lamaddalena, N., Coppola, A., 2022. A bimodal extension of the ARYA&PARIS approach for predicting hydraulic properties of structured soils. J. Hydrol. 610, 127980. https://doi.org/10.1016/j.jhydrol.2022.127980.

Heller, O., 2026. Data set]. *Zenodo*. Dataset Softw. Support. " Energy-Based Model. Soil. Fragm. Tillage. https://doi.org/10.5281/zenodo.18525965.

Hevia, Graciela G., Mendez, Mariano, Buschiazzo, Daniel E., 2007. Tillage affects soil aggregation parameters linked with wind erosion. Geoderma 140 (1–2), 90–96. https://doi.org/10.1016/j.geoderma.2007.03.001.

Huntington, T.G., Johnson, C.E., Johnson, A.H., Siccama, T.G., Ryan, D.F., 1989. Carbon, organic matter, and bulk density relationships in a forested spodosol. Soil. Sci. 148 (5), 380–386.

Jarvis, N., Coucheney, E., Lewan, E., Klöffel, T., Meurer, K.H.E., Keller, T., Larsbo, M., 2024. Interactions between soil structure dynamics, hydrological processes, and organic matter cycling: a new soil-crop model. Eur. J. Soil. Sci. 75 (2), e13455. https://doi.org/10.1111/ejss.13455.

Jurin, James, 1719. An account of some new experiments, relating to the action of glass tubes upon water and quicksilver. Philos. Trans. R. Soc. Lond. 30, 1083–1096. https://doi.org/10.1098/rstl.1717.0070.

Keller, Thomas, Arvidsson, Johan, Dexter, Anthony R., 2007. Soil structures produced by tillage as affected by soil water content and the physical quality of soil. Soil. Tillage Res. 92 (1), 45–52. https://doi.org/10.1016/j.still.2006.01.001.

Keller, Thomas, Dexter, Anthony R., 2012. Plastic limits of agricultural soils as functions of soil texture and organic matter content. Soil. Res. 50 (1), 7–17. https://doi.org/10.1071/SR11174.

Knadel, Maria, Ur Rehman, Hafeez, Pouladi, Nastaran, Wollesen de Jonge, Lis, Moldrup, Per, Arthur, Emmanuel, 2021. Estimating atterberg limits of soils from reflectance spectroscopy and pedotransfer functions. Geoderma 402 (ember), 115300. https://doi.org/10.1016/j.geoderma.2021.115300.

König, S., Weller, U., Betancur-Corredor, B., Lang, B., Reitz, T., Wiesmeier, M., Wollschläger, U., Vogel, H.-J., 2023. BODIUM—A systemic approach to model the dynamics of soil functions. Eur. J. Soil. Sci. 74 (5), e13411. https://doi.org/10.1111/ejss.13411.

Krabbe, W., 1958. "Über die Schrumpfung bindiger Böden. Mitt. der Vers. F. üR. Grund. - und Wasserbau der Tech. Hochsch. Hann. 13, 256–342.

Kuipers, H., 1963. The objectives of soil tillage; introduction to the conference-theme. Neth. J. Agric. Sci. 11 (2), 91–96. https://doi.org/10.18174/njas.v11i2.17553.

Leij, Feike J., Ghezzehei, Teamrat A., Or, Dani, 2002. Analytical models for soil pore-size distribution after tillage. Soil. Sci. Soc. Am. J. 66 (4), 1104–1114. https://doi.org/10.2136/sssaj2002.1104.

Lu, Ning, 2020. Unsaturated soil mechanics: fundamental challenges, breakthroughs, and opportunities. J. Geotech. Geoenviron. Eng. 146 (5), 02520001. https://doi.org/10.1061/(ASCE)GT.1943-5606.0002233.

Maharjan, G.R., Prescher, A.K., Nendel, C., Ewert, F., Mboh, C.M., Gaiser, T, T., Seidel, S. J., 2018. Approaches to model the impact of tillage implements on soil physical and nutrient properties in different agro-ecosystem models. Soil. Tillage Res. 180, 210–221. https://doi.org/10.1016/j.still.2018.03.009.

Manrique, L.A., Jones, C.A., 1991. Bulk density of soils in relation to soil physical and chemical properties. Soil. Sci. Soc. Am. J. 55 (2), 476. https://doi.org/10.2136/sssaj1991.03615995005500020030x.

Men, M.X., Peng, Z.P., Hao, X., Yu, Z.R., 2008. "Investigation on pedotransfer function for estimating soil bulk density in Hebei Province.". Chin. J. Soil. Sci. 1, 20.

Mucha, Dorota, Wójcik, Emilia, 2013. Testing shrinkage factors: comparison of methods and correlation with index properties of soils. Bull. Eng. Geol. Environ. 72 (1), 15–24. https://doi.org/10.1007/s10064-012-0449-0.

Müller, L., Lipiec, J., Kornecki, T.S., Gebhard, S., 2011. Trafficability and workability of soils. Encyclopedia of agrophysics. Springer, Dordrecht, pp. 912–924. https://doi.org/10.1007/978-90-481-3585-1_176.

Munkholm, Lars J., Per, Schjønning, Bev, D.Kay, 2002. Tensile strength of soil cores in relation to aggregate strength, soil fragmentation and pore characteristics. Soil. Tillage Res. 64 (1), 125–135. https://doi.org/10.1016/S0167-1987(01)00250-1.

Obour, P.B., Lamandé, M., Edwards, G., Sørensen, C.G., Munkholm, L.J., 2017. Predicting soil workability and fragmentation in tillage: a review. Soil. Use Manag. 33 (2), 288–298. https://doi.org/10.1111/sum.12340.

Ojeniyi, S.O., Dexter, A.R., 1979a. Soil factors affecting the macro-structures produced by tillage. Trans. ASAE 22 (2), 339–0343. https://doi.org/10.13031/2013.35016.

Ojeniyi, S.O., Dexter, A.R., 1979b. Soil structural changes during multiple pass tillage. Trans. ASAE 22 (5), 1068–1072. https://doi.org/10.13031/2013.35157.

Or, D., Ghezzehei, T.A., 2002. Modeling post-tillage soil structural dynamics: a review. Soil. Tillage Res. 64, 41–59. https://doi.org/10.1016/S0167-1987(01)00256-2.

Or, Dani, Keller, Thomas, Schlesinger, William H., 2021. Natural and managed soil structure: on the fragile scaffolding for soil functioning. Soil. Tillage Res. 208, 104912. https://doi.org/10.1016/j.still.2020.104912.

Perfect, E., Kay, B.D., Ferguson, J.A., da Silva, A.P., Denholm, K.A., 1993. Comparison of functions for characterizing the dry aggregate size distribution of tilled soil. Soil. Tillage Res. 28 (2), 123–139. https://doi.org/10.1016/0167-1987(93)90022-H.

Petelkau, H., 1984. Auswirkungen von schadverdichtungen auf bodeneigenschaften und *Pflanzenertrag* sowie Massnahmen zu ihrer Minderung. Grundlagen und verfahren der rationellen bodenbearbeitung und erschliessung des unterbodens fuer pflanzen. Akad. der Landwirtsch. der DDR Tag. 215, 39–48.

R Core Team (2026). R: A Language and Environment for Statistical Computing. R Foundation for Statistical Computing, Vienna, Austria. https://www.R-project.org/.

Roytburg, E., Chaplin, J., 1995. Stochastic modeling of soil condition during tillage. Site-specific Management for Agricultural Systems. John Wiley; Sons, Ltd, pp. 581–599. https://doi.org/10.2134/1995.site-specificmanagement.c43.

Salimi, Kwestan, Cerato, Amy B., Vahedifard, Farshid, Miller, Gerald A., 2021. General model for the uniaxial tensile strength characteristic curve of unsaturated soils. J. Geotech. Geoenviron. Eng. 147 (7), 04021051. https://doi.org/10.1061/(ASCE)GT.1943-5606.0002567.

Terzaghi, Karl, 1943. Theoretical soil mechanics. John Wiley; Sons, Inc. https://doi.org/10.1002/9780470172766.

Tomasella, Javier, Hodnett, Martin G., 1998. Estimating soil water retention characteristics from limited data in Brazilian Amazonia. Soil. Sci. 163 (3), 190–202.
Unger, P.W., D.M. van Doren, F.D. Whisler, and E.L. Skidmore, eds. 1982. *Predicting Tillage Effects on Soil Physical Properties and Processes*. ASA Special Publication No. 44. 677 South Segoe Road, Madison, Wisconsin 53711: American Society of Agronomy; Soil Science Society of America. doi:10.2134/asaspecpub44.
Van Genuchten, M.T., 1980. A closed-form equation for predicting the hydraulic conductivity of unsaturated soils. Soil. Sci. Soc. Am. J. 44 (5), 892–898. https://doi.org/10.2136/sssaj1980.03615995004400050002x.
Vdovenko, D., Leuther, F., Diamantopoulos, E., 3–8 May 2026. Modeling the effects of soil structure dynamics on soil hydraulic properties. EGU General Assembly 2026, Vienna, Austria, EGU26-1244. https://doi.org/10.5194/egusphere-egu26-1244.
Williams, J.R., Jones, A.C., Dyke, T.P., 1984. A modeling approach to determining the relationship between erosion and soil productivity. Trans. ASAE 27 (1), 129–0144. https://doi.org/10.13031/2013.32748.
Wösten, J.H.M., Lilly, A., Nemes, A., Le Bas, C., 1999. Development and use of a database of hydraulic properties of European soils. Geoderma 90 (3–4), 169–185. https://doi.org/10.1016/s0016-7061(98)00132-3.